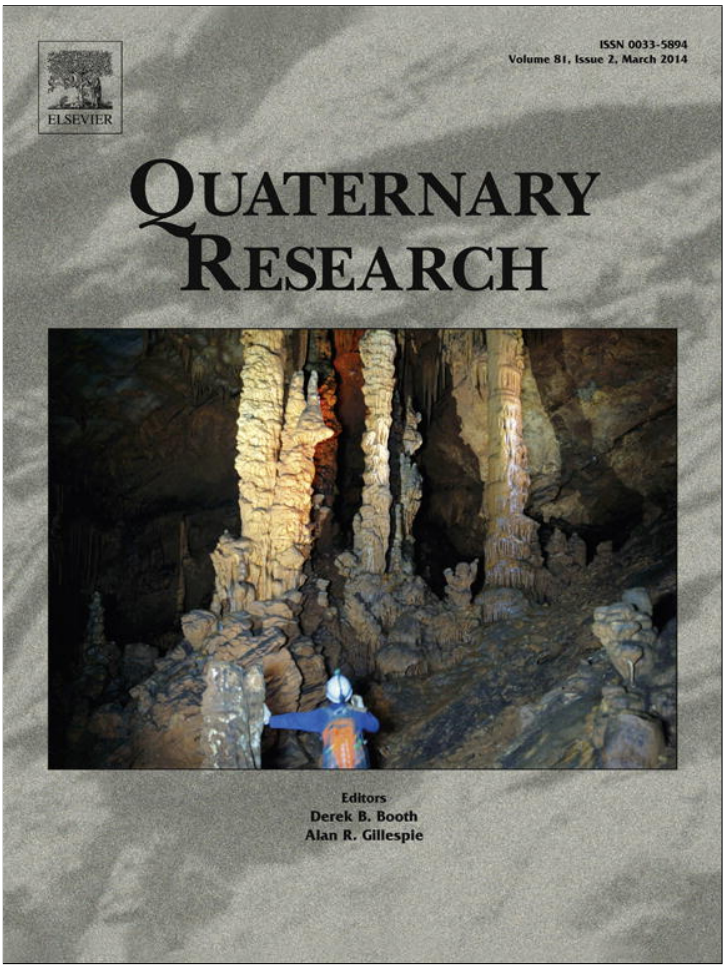

Quaternary Research 81 (2014) 381–391

Contents lists available at ScienceDirect

Quaternary Research

journal homepage: www.elsevier.com/locate/yqres

Several distinct wet periods since 420 ka in the Namib Desert inferred from U-series dates of speleothems

Mebus A. Geyh [a,*], Klaus Heine [b]

[a] University of Marburg, Germany
[b] Institute of Geography, Regensburg University, Germany

ARTICLE INFO

Article history:
Received 8 April 2013
Available online 9 January 2014

Keywords:
Namib Desert
Speleothems
^{230}Th/U dating
Middle/Late Pleistocene
Paleoclimate
Paleoprecipitation
Milankovitch forcing

ABSTRACT

The scarcity of numerical dates of the arid areas in southern Africa is a challenge for reconstructing paleoclimate. This paper presents a chronological reconstruction in the central part of the Namib Desert, Namibia, for the last 420,000 yr. It is based on ^{230}Th/U dates (TIMS) from a large stalagmite and a thick flowstone layer in a small cave located in the hyper-arid central Namib Desert. The results provide for the first time evidence of three or possibly four succeeding wet periods of decreasing intensity since 420 ka through which speleothem deposited at approximately 420–385 ka, 230–207 ka and 120–117 ka following the 100-ka Milankovitch cycle. Speleothem growth was not recorded for the Holocene. These wet periods interrupted the predominantly dry climate of the Namib Desert and coincided with wet phases in deserts of the northern hemisphere in the Murzuq Basin, Sahara, the Negev, Israel, the Nafud Desert, Saudi Arabia, and the arid northern Oman, Arabian Peninsula.

Introduction

Numerically dated long-term paleoclimatic records of the deserts in southern Africa, since the middle Pleistocene, are not yet available due to the scarcity of datable material. In the arid and semi-arid regions of the Namib Desert, rudimentary paleoclimatic knowledge from this period is based on a few ^{230}Th/U dates of speleothems covering the last two marine oxygen isotope stages (Heine, 1991, 1998; Brook et al., 1996). Absolute chronologies are required to find correlations between wet periods in the deserts of the northern and southern hemispheres, between terrestrial and marine sedimentation and between erosion processes with rainfall in southern Africa and with sea surface temperatures (SSTs) of the Benguela Current. New terrestrial information is important, because the reconstruction of the Quaternary paleoclimate presently based on the mineralogy, chemistry and the microfossil content of marine sediments off the southwestern African coast have yielded ambiguous results (e.g., Little et al., 1997; Stuut et al., 2002, 2011; Wefer et al., 2004; Pichevin et al., 2005; Collins 2011).

In this study we established an absolute ^{230}Th/U chronology of cave calcite (speleothem) for the last 420 ka from the central Namib Desert. These Namib speleothems provided information on wet periods during the dominant arid climate of the Middle and Late Pleistocene, because availability of drip water is the dominant factor controlling speleothem formation (e.g., Geyh and Franke, 1970). Previously, little was known about the timing, variability and the intensity of wet phases in the Namib Desert beyond the radiocarbon timescale. Absolute chronologies of speleothems supplement the reconstruction of terrestrial temperature changes deduced from stable isotope oxygen compositions of deep-sea sediments and ice cores, by adding records of moisture changes. The main objectives of this study were to reveal whether the speleothems of the cave formed during glacial or interglacial periods, whether relatively long-lasting wet periods occurred and if so, did they coincide with the known wet periods in deserts of the northern hemisphere.

Settings of the Namib cave

The Namib Desert (Fig. 1) is one of the oldest deserts in the world (Vermeesch et al., 2010; Ward et al., 1983) and extends over ~150 km across the coastal plain of southwestern Africa between the southern Atlantic Ocean and the base of the Great Escarpment at about 1000 m asl with an average slope of 0.3–0.5°. The central Namib Desert is composed of Proterozoic metamorphic rocks with granitic intrusives. It is a flat landscape (Namib Unconformity Surface, Ollier, 1977) with inselbergs, resistant dolerite and marble ridges and some deeply incised canyons of ephemeral rivers (Van der Wateren and Dunai, 2001). Since the Miocene, the Namib Desert has experienced increasing aridity (Partridge and Maud, 1987). Heine (1992) hypothesizes that Namib caves developed during Miocene pluvial phases. The last long-term period of soil formation with warm and seasonally humid climate ended about 10 Ma ago. Subsequently the Namib-

* Corresponding author at: Rübeland 12, 29308 Winsen (Aller), Germany. Tel.: +49 5146 987123.
E-mail address: mebus.geyh@t-online.de (M.A. Geyh).

0033-5894/$ – see front matter
http://dx.doi.org/10.1016/j.yqres.2013.10.020

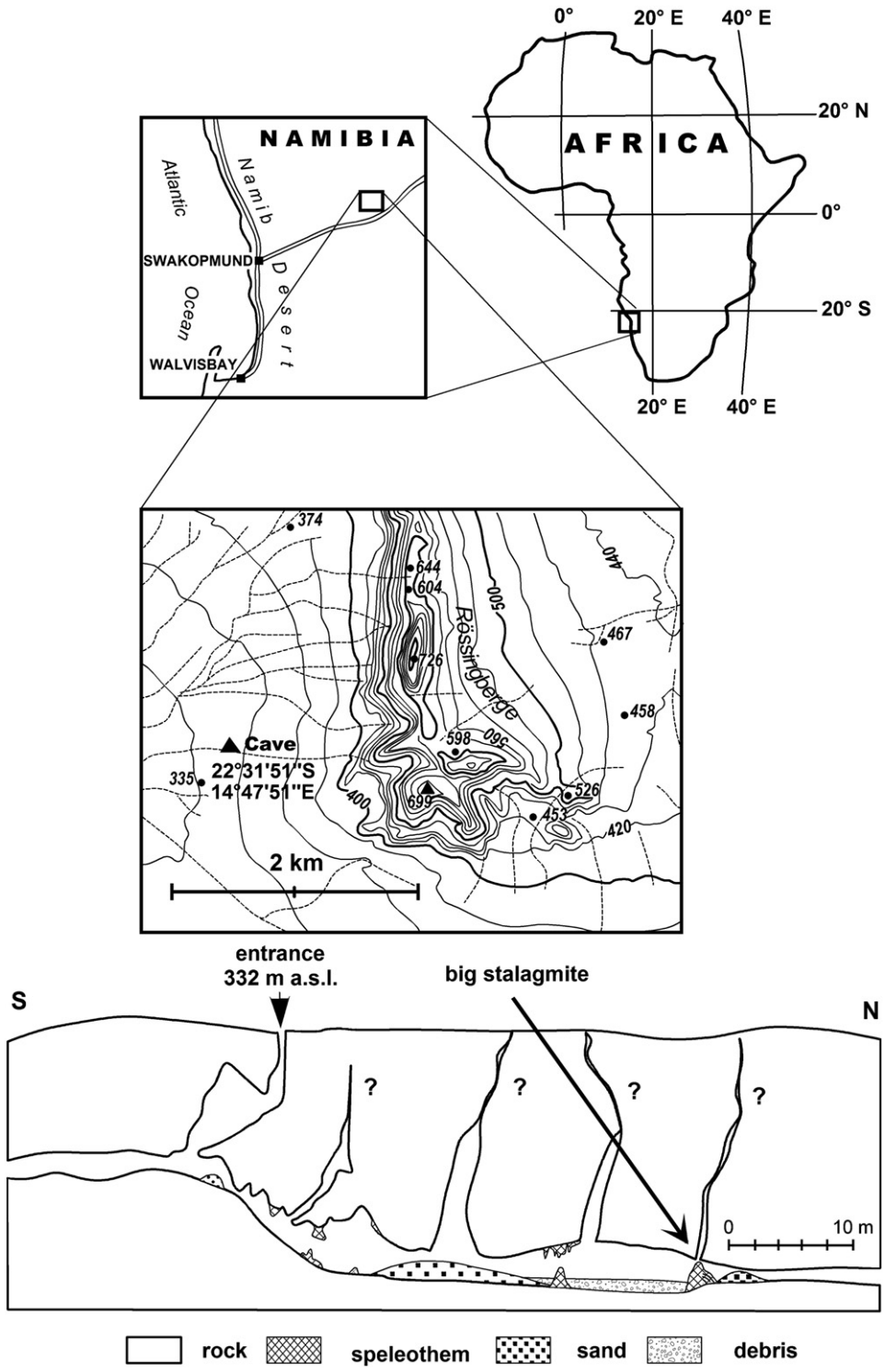

Figure 1. Location map of the study area and section of the Rössing Cave.

Desert Phase ('Namib-Wüsten-Phase') (Besler et al., 1994) commenced building up the Namib Erg (Vermeesch et al., 2010). This process was caused by the onset of the cold Benguela Current off the southwestern African coast as a result of the growing eastern Antarctic ice sheet. During the Neogene, only a few wet periods interrupted the dominating hyper-arid climate. They were characterized by savanna vegetation with soil formation (acrisols, ferrasols) on the Namib Unconformity Surface. Plants disappeared and soils became eroded when the climate became again more arid. Then calcisols and gypsisols with hard crusts developed (e.g., Yaalon and Ward, 1982). The gypcretes of the central Namib Desert document missing major wet phases since at least 100 ka (Heine and Walter, 1996). At present, the Namib Desert is one of the driest areas worldwide.

The geologist Ernst Jaspers discovered the Rössing Cave in the Namib Desert in the late 20th century. This cave is located at 14°47′51″ E and 22°31′51″ S (332 m asl) near the Rössing Mountains within a narrow ridge of marble stretching parallel to the NNW/SSE direction of folded Neoproterozoic pegmatite, granite, quartzite and marble. About 100 m

to the east and west of the cave, two faults run parallel to the marble ridge emerging a few meters above the rock-cut and gravel-veneered plain of the Namib Desert. The ridge is a hydraulic barrier for the runoff from the Rössing Mountains to the east.

The cave entrance is situated within interbedded bands of calc-silicate rock. The accessible part of the cave has three chambers located 10–20 m beneath the surface. Their width and length range from a few meters to a maximum of 15 m and from 10 to 25 m, respectively; their height ranges from several decimeters to 3 m. Most of the cave voids might have formed during the Miocene (Heine, 1992) by phreatic flow or at least intermittent running water under humid climatic conditions documented by water-level notches and grooves on the cave walls. On the cave floor, breakdown materials and eolian blown-in sand cones underneath fissures are found at some places. At present, the cave is dry, albeit drops of seeping water from the roof have been after heavy rains (Jaspers E., personal communication, 1978). The present catchment of the cave extends over an area of a few km^2.

Several kinds of dripstone and flowstone, such as small stalactites, cave drapery and popcorn are distributed over the Rössing Cave. The sampled speleothems consisted of one big stalagmite (ca. 90 cm high, ca. 60 and 40 cm thick in the lower and upper parts, respectively) and a thick flowstone layer at the base of its southern flank. The stalagmite formed beneath a fissure (Fig. 2) through which drip water and fine eolian sand entered the cave.

At present, the central Namib Desert receives on average 5–18 mm rain per yr (Mendelsohn et al., 2002; Eckardt et al., 2013). The combination of cool air masses under the influence of the cold Benguela Current together with high-pressure conditions in the subtropics is mainly responsible for the aridity of the Namib Desert. Occasional rain mainly comes with the summer monsoon approaching from the distant Indian Ocean. Besides rainfall, fog, including advected fog, coastal stratus clouds, high stratus clouds, radiation fog and fog drizzle (Eckardt et al., 2013) are important moisture sources in the Namib Desert and may considerably exceed that of actual rainfall on inselbergs and rock outcrops (Lancaster et al., 1984). However, fog does not form drip water in the cave.

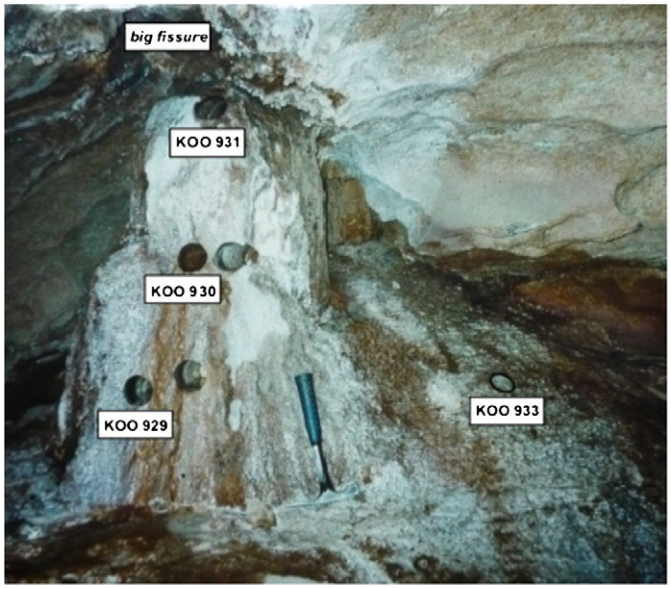

Figure 2. Five horizontally drilled cores were taken from the ca. 90 cm high and 40–60 cm-thick stalagmite in the Roessing Cave from which three (KOO 929–931) were used for $^{230}Th/U$ dating. The vertical core KOO 933 was taken from the flowstone right at the base of the stalagmite.

Sampling and methods

Speleothem samples for $^{230}Th/U$ dating were collected with a Hilti-DD 100 Diamond-Corer. Coring was done with distilled water. Five horizontal cores with a diameter of 6.3 cm and a maximum length of 40 cm were obtained from the stalagmite at 28 cm above the base (L = lower core, KOO 929), at 54 cm (M = middle core, KOO 930) and at 88 cm, near the top (T = upper core, KOO 931). One vertical core was drilled in the flowstone (F = flowstone core, KOO 933) surrounding the southern and eastern base of the stalagmite (Fig. 2). Because the top of the stalagmite reached the ceiling of the cave, vertical coring was not possible, even though it was thought to be desirable. 47 samples were cut from the cores (Table 1). Two samples (M 1.1 and M 1.2) were collected with a hammer from the outer 3 cm rim layer close to the middle core.

The vertical growth layers of the stalagmite were reconstructed referring to all cores (Fig. 3) in order to correlate the sampling positions with each other. At the beginning, the stalagmite probably formed in the common manner by superposition of cap-like carbonate layers (M21–M25). When it reached the wall on the rear side the drip water could only flow along the front side and deposited near-vertical calcite layers. Therefore, contrary to vertical grown stalagmites the applied horizontal coring promised more temporal information than vertical coring. The age should increase from the rim towards the center of the stalagmite. The cores represented differing formation phases reflected in the laminations of both, clean bright carbonate and impure colored carbonate with varying contents of sands and debris. Non-calcareous inclusions caused the coloring layers. In the outermost part of the stalagmite, vertical solution-etched grooves developed prior to the formation of the youngest, less than 1–3 cm thick set of very thin calcite bands (M 1.1 and M 1.2).

The vertical core of the flowstone was horizontally laminated (Fig. 4). The upper part consisted of dirty and sandy limestone. The middle part was heavily corroded, porous with iron incrustations and had a very low mechanical stability. The base of this core was compact, whitish and only slightly porous.

All cores were cut along their axis into two halves from which 47 slices of 1–2 mm thickness and 5–10 mm length were taken for $^{230}Th/U$ age determinations. Stratigraphically, the location of sampling sites was guided by such properties as color change. The required sample quantity was small due to the unusually large uranium concentration up to 10,120 ppb.

The thermal ionization mass spectrometric (TIMS) analyses were performed on 0.2–0.9 g material. The samples were dissolved in a HNO_3/HCl mixture applying the total dissolution technique (Bischoff and Fitzpatrick, 1991; Ivanovich and Harmon, 1992; Kaufman, 1993). A ^{229}Th and a $^{233}U/^{236}U$ double spike were added and the leach solution equilibrated. Uranium and thorium were separated by co-precipitation with $Fe(OH)_3$ before their separation and purification by ion-exchange chromatography. The uranium and thorium fractions were loaded on rhenium filaments and their isotopic ratios were measured with the mass spectrometer (Finnigan MAT 262, equipped with a quadruple device — RPQ filter).

According to the principles of $^{230}Th/U$ dating method uranium is deposited together with the secondary carbonate. Radioactive decay of ^{234}U und ^{238}U forms the daughter isotopes $^{230}Th^*$ and ^{234}U, respectively. Therefore, the $^{230}Th^*/^{234}U$ and $^{234}U/^{238}U$ activity ratios (AR) are the main parameters for the calculation of the $^{230}Th/U$ age t. The change of both the $^{234}U/^{238}U$ AR and $^{230}Th^*/^{238}U$ AR with increasing age of the sample which fulfills these requirements is shown in the isotope-ratio evolution plot (Fig. 5) developed by Kaufman and Broecker (1965). Each initial $^{234}U/^{238}U$ AR yields a separate evolution line. All these lines meet the point (1,1) at radioactive equilibrium corresponding to an infinite age. The ARs of coeval samples fit more-or-less straight lines of their corresponding ages, which are termed “isochrones.”

Table 1
Results of ^{230}Th/U analyses and dating.

Code TIMS	speleothem	properties	Depth	U	Th	[^{230}Th]	^{230}Th/^{232}Th	^{230}Th/^{234}U	^{234}U/^{238}U	^{230}Th/U age	^{230}Th/U age	^{230}Th/U age
			cm	conc.	conc.	act.	AR	AR	AR	uncorr.	corr.	oldest
				ppb	ppb	dph/g				ka	ka	ka
KOO 933 (flowstone)												
F01	2236	Porous, dirty, compact	0.2	2270	1473	83	5	0.6972 ± 0.0036	1.1740 ± 0.0072	124	117 ± 3	510
F02	2271	Porous, dirty, compact	0.5	2090	2503	78	2	0.7198 ± 0.0061	1.1628 ± 0.0026	132	118 ± 5	510
F03	2272	Porous, dirty, Compact	0.8	2240	1676	81	3	0.7088 ± 0.0025	1.1550 ± 0.0022	129	120 ± 3	615
F04	2270	Very compact	2.5	2720	117	120	70	0.8842 ± 0.0027	1.1218 ± 0.0010	215	208 ± 2	640
F05	*2305*	*Compact*	*3.8*	*5010*	*457*	*282*	*42*	*1.0633 ± 0.0021*	*1.1885 ± 0.0028*	*Open system*		
F06	2483	Porous, iron deposits	4.2	1550	209	69	23	0.9096 ± 0.0041	1.1022 ± 0.0018	238	211 ± 6	590
F07	2306	Compact, porous	4.8	4260	368	191	35	0.8839 ± 0.0056	1.1386 ± 0.0026	212	199 ± 5	560
F08	2269	Compact, light, above iron	6.3	1960	276	94	23	0.9492 ± 0.0025	1.1363 ± 0.0014	270	233 ± 3	650
F09	2484	Compact, white	8.2	5340	7	246	241	0.9098 ± 0.0022	1.1394 ± 0.0021	231	230 ± 2	625
F10	2235	Compact, light brown	10.0	1370	235	68	20	0.9499 ± 0.0027	1.1704 ± 0.0026	264	223 ± 3	610
F11	*2307*	*Crystalline, porous*	*13.2*	*1490*	*2028*	*79*	*3*	*1.0960 ± 0.0048*	*1.0873 ± 0.0013*	*Open system*		
F12	2234	Light brown, compact	17.2	3080	2	137	5590	0.9832 ± 0.0066	1.0166 ± 0.0044	412	413^{+47}_{-32}	510
F13	2233	Light, compact	22.2	5120	23	229	676	0.9788 ± 0.0026	1.0258 ± 0.0019	382	381 ± 11	605
KOO 931 (upper core)												
U01	2242	Dark brown, laminated	11.2	5910	79	269	234	0.9850 ± 0.0011	1.0398 ± 0.0014	387	387 ± 6	660
U02	*2241*	*White laminated*	*17.1*	*1100*	*11*	*57*	*344*	*1.0982 ± 0.0057*	*1.0593 ± 0.0051*	*Open system*		
U03	2240	Light brown	24.7	6540	2	297	1012	0.9853 ± 0.0023	1.0384 ± 0.0026	390	390 ± 12	590
U04	2239	Dark brown, porous (?)	33.2	5760	128	257	137	0.9738 ± 0.0024	1.0280 ± 0.0026	363	363 ± 10	580
KOO 930 (middle core)												
M1.1	990	Dark brown	1.5	4058	294	141	33	0.6912 ± 0.0086	1.1290 ± 0.0053	124	121 ± 3	425
M1.2	991	Dark brown	2.5	6095	358	244	47	0.8692 ± 0.0112	1.0376 ± 0.0044	216	213 ± 9	403
M01	*2100*	*Middle brown, laminated*	*5.3*	*5470*	*114*	*249*	*149*	*0.9823 ± 0.0031*	*1.0422 ± 0.0012*	*376*	*376 ± 12*	*400*
M02	2099	Middle brown, laminated	5.6	4280	157	194	85	0.9834 ± 0.0015	1.0382 ± 0.0009	383	382 ± 6	700
M03	*2098*	*Middle brown, laminated*	*5.9*	*4680*	*31*	*214*	*465*	*0.9874 ± 0.0027*	*1.0408 ± 0.0011*	*395*	*395 ± 12*	*620*
M04	*2097*	*Middle brown above white*	*7.4*	*5140*	*26*	*223*	*583*	*0.9387 ± 0.0810*	*1.0408 ± 0.0027*	*286*	*>280*	*280*
M05	2096	Dark brown, laminated	9.2	5550	71	252	240	0.9863 ± 0.0024	1.0343 ± 0.0027	399	398 ± 14	584
M06	*2095*	*Dark brown*	*11.1*	*4910*	*176*	*388*	*151*	*1.7044 ± 0.0022*	*1.0408 ± 0.0012*	*Open system*		
M07	2110	Dark brown and white	11.4	4770	225	214	65	0.9747 ± 0.0031	1.0335 ± 0.0046	362	362 ± 14	530
M08	*2094*	*Dark brown*	*11.7*	*10120*	*358*	*264*	*50*	*0.5671 ± 0.0006*	*1.0325 ± 0.0012*	*91*	*89 ± 1*	*680*
M09	2111	Light brown	12.7	3820	4	175	3354	0.9934 ± 0.0054	1.0361 ± 0.0014	428	428^{+35}_{-27}	570
M10	*2112*	*Beige*	*13.6*	*2880*	*5*	*132*	*1927*	*1.0047 ± 0.0086*	*1.0239 ± 0.0044*	*>500*	*>500*	*500*
M11	2113	White	14.2	2410	14	109	528	0.9850 ± 0.0150	1.0340 ± 0.0008	465	394^{+83}_{-47}	465
M12	*2157*	*Beige*	*15.3*	*4250*	*12*	*193*	*1152*	*0.9932 ± 0.0013*	*1.0307 ± 0.0013*	*437*	*437 ± 10*	*660*
M13	*2158*	*White*	*16.0*	*2270*	*13*	*106*	*575*	*1.0088 ± 0.0029*	*1.0372 ± 0.0012*	*Open system*		
M14	*2159*	*White, laminated*	*17.3*	*3420*	*254*	*252*	*68*	*1.5981 ± 0.8790*	*1.0396 ± 0.0009*	*Open system*		
M15	2160	Middle brown	19.2	4550	7	207	2067	0.9884 ± 0.0018	1.0342 ± 0.0020	408	408 ± 11	615
M15a	*2470*	*White*	*19.2*	*4846*	*14*	*0*	*2*	*01.0025 ± 0.0160*	*1.0399 ± 0.0029*	*478*	*>465*	*465*
M16	2137	White	21.3	2900	3	133	3183	1.0003 ± 0.0012	1.0329 ± 0.0013	480	480 ± 15	660
M17	*2468*	*White*	*21.3*	*3080*	*4*	*109*	*2576*	*1.0214 ± 0.0047*	*1.0427 ± 0.0028*	*Open system*		
M17a	*2471*	*Beige*	*21.7*	*8050*	*6*	*0*	*223*	*1.0305 ± 0.0465*	*1.0130 ± 0.0024*	*>400*	*>364*	*364*
M18	*2469*	*Beige*	*22.6*	*9730*	*8*	*429*	*3984*	*0.9706 ± 0.0268*	*1.0216 ± 0.0023*	*>400*	*>400*	*400*
M19	2349	Dark brown above white	24.0	8810	1	399	2718	0.9838 ± 0.0056	1.0338 ± 0.0064	389	389^{+33}_{-25}	490
M20	2482	Dark brown above white	24.0	8050	1	368	2615	0.9898 ± 0.0030	1.0386 ± 0.0031	407	407 ± 18	570
M21	2165	Light brown	25.8	8860	2	403	1477	0.9855 ± 0.0033	1.0386 ± 0.0035	390	390 ± 18	560
M22	2201	Light brown, iron red	27.7	4430	229	198	59	0.9702 ± 0.0064	1.0365 ± 0.0018	347	347 ± 18	550
M23	*2138*	*Light brown*	*29.8*	*4780*	*2*	*243*	*7883*	*1.1202 ± 0.0943*	*1.0209 ± 0.0026*	*Open system*		
M24	*2166*	*Light brown, laminated*	*33.0*	*5230*	*8*	*233*	*2076*	*0.9834 ± 0.0028*	*1.0174 ± 0.0014*	*411*	*411 ± 16*	*620*
M25	*2167*	*White*	*35.1*	*4230*	*8*	*188*	*1557*	*0.9805 ± 0.0025*	*1.0187 ± 0.0018*	*398*	*398 ± 13*	*550*
M26	*2168*	*Dark brown*	*37.3*	*5510*	*2*	*240*	*7971*	*0.9582 ± 0.0392*	*1.0233 ± 0.0016*	*328*	*328 ± 63*	*360*
M27	*2139*	*Dark brown, white, doted*	*38.7*	*5700*	*2*	*252*	*8966*	*0.9766 ± 0.0040*	*1.0173 ± 0.0024*	*385*	*385 ± 19*	*590*
KOO 929 (lower core)												
L01	2237	Dark brown, laminated	1.5	4130	12	190	1065	0.9836 ± 0.0019	1.0527 ± 0.0023	369	369 ± 8	610
L02	2243	White, laminated	12.5	2680	7	124	1202	0.9977 ± 0.0022	1.0430 ± 0.0025	439	439 ± 18	600
L03	*2238*	*White, laminated*	*17.1*	*3600*	*12*	*169*	*1006*	*1.0101 ± 0.0096*	*1.0443 ± 0.0019*	*Open system*		

Explanations: code — sample code of the submitter; TIMS — laboratory code of TIMS dating; depth — distance in centimeters from the surface of both the flowstone and stalagmite cores; [^{230}Th] act. — specific ^{230}Th activity in disintegrations per hour and per g of sample; uncorr. — ^{230}Th/U age; corr. — ^{230}Th/U age corrected for detrital ^{230}Th; oldest — oldest determinable ^{230}Th/U age; outliers — data in italics.

Under natural conditions, deviations may occur from the mentioned principles of ^{230}Th/U dating, when e.g. detrital clay with thorium isotopes is deposited on the surface of the speleothem during its growth. This detrital (unsupported) thorium has an initial $^{230}Th^{+}/^{232}Th_o$ AR (also called initial Th_o index = f_o. The measured present-day Th index is termed f). This unsupported $^{230}Th^{+}$ of the detritus Th decays, while the activity of the supported $^{230}Th^{*}$ of the sample increases. The activity of $^{230}Th^{*}$ required for the ^{230}Th/U dating is calculated from both the measured total $^{230}Th_{total}$ activity ($=Th^{*} + Th^{+}$) and the ^{232}Th activity of the sample using Eq. (1) (Kaufman and Broecker, 1965), assuming binary mixing of Th^{*} and Th^{+}.

$$\left[^{230}Th^{*}\right] = \left[^{230}Th_{total}\right] - \left[\frac{^{230}Th^{+}}{^{232}Th}\right]_0 e^{-\lambda_{230}\cdot t} \cdot \left[^{232}Th\right] = \left[^{230}Th_{total}\right] - f \cdot \left[^{232}Th\right]. \quad (1)$$

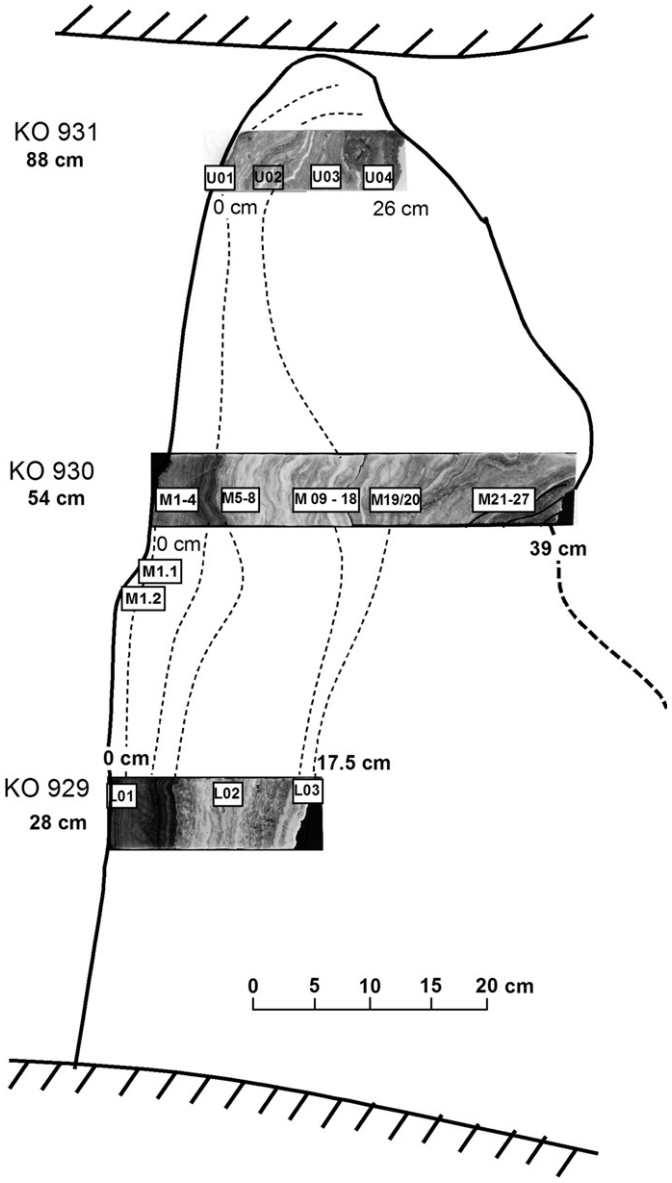

Figure 3. Reconstructed growth lines (dashed) of the stalagmite with superimposed copies of the cores. The given sampling depth of each core (Table 1) refers to the surface of the stalagmite.

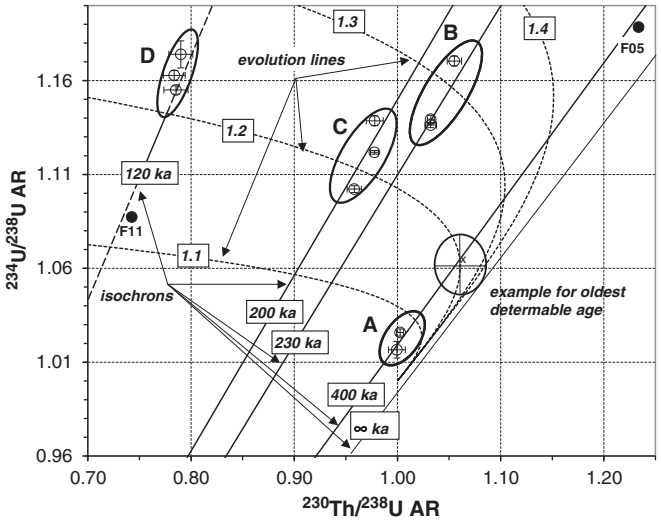

Figure 5. Isotope-ratio evolution plot of the $^{230}Th/^{238}U$ AR and $^{234}U/^{238}U$ AR (Kaufman and Broecker, 1965): Any initial $^{234}U/^{238}U$ yields an individual evolution line. All meet the point (1,1) at radioactive equilibrium corresponding to an infinite age. Coeval samples plot on more-or-less straight lines termed "isochrones." The circle with the internal crux touching the "isochron" of the infinite age (artificial date) elucidates the conception of the determination the oldest datable $^{230}Th/U$ ages (Geyh, 2008). The detritus-corrected data for the flowstone KOO 933 shows a good fit with the isochrons of 400 ka (A), 230 ka (B), 200 ka (C) and 120 ka (D) and plot within the evolution curves of initial $^{234}U/^{238}U$ ARs between 1.4 and 1.1. The samples F05 and F11 (filled black dots) reflect disturbed isotopic U/Th systems. The apparently old sample F05 was taken from the young rim layer and the apparently young sample F11 was collected from the base of the flowstone.

If the measured $^{230}Th/^{232}Th$ AR is > 10 the age correction is negligible (Table 1).

The initial ^{234}U activity $[^{234}U_0]$ at the time of sinter formation is calculated from the measured ^{234}U activity $[^{234}U]$ (Table 1) by Eq. (2):

$$\left[^{234}U_0\right] = 1 + \left(\left[^{234}U\right] - 1\right) \cdot e^{\lambda_{234} \cdot t}. \quad (2)$$

In order to check whether binary mixing describes the thorium und uranium isotope compositions, Rosholt (1976) and Osmond et al. (1970) developed plots for couples of thorium/uranium isotope activity ratios. All used data have to fit straight lines which are termed "isochrons" (Kaufman and Broecker, 1965; Ku and Liang, 1984; Bischoff

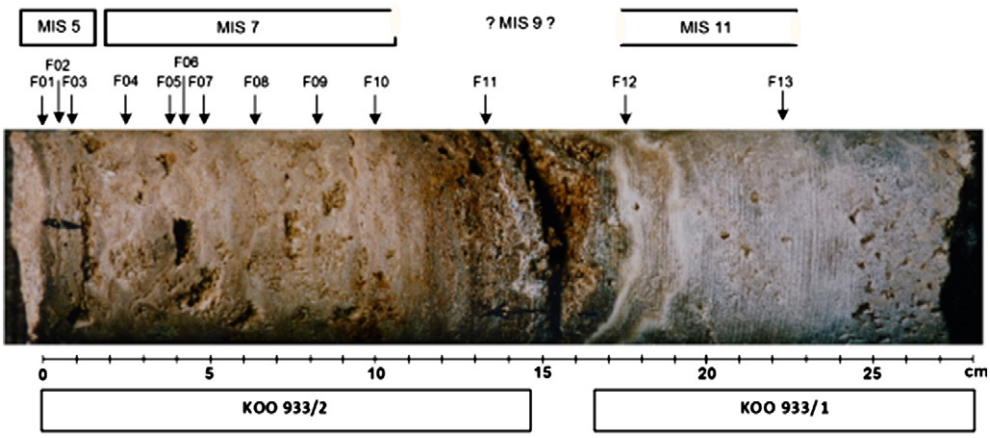

Figure 4. Core KOO 933 with sampling locations and the corresponding ranges of $^{230}Th/U$ ages. The sample F01 represents the surface of the flowstone.

and Fitzpatrick, 1991; Scholz and Hoffmann, 2008). If this prerequisite is not fulfilled the case of disturbed U and Th isotope compositions is identified which is often caused by uranium dissolution or accumulation (open system conditions with respect to uranium).

Rosholt used for his plots I and II the $^{230}Th/^{232}Th$ and $^{234}U/^{232}Th$ ARs as numerators, respectively, and the $^{238}U/^{232}Th$ AR as common denominator. The Rosholt I plot is most frequently used as the slope of the "isochron" equals the $^{230}Th^{*}/^{234}U$ AR which is the most important age-dependent parameter for the calculation of the $^{230}Th/U$ age. The intercept of the "isochron" with the Y axis equals to the present-day initial $^{230}Th^{+}/^{232}Th$ AR used for the detritus correction (Eq. (1)). The slope of the "isochron" of the Rosholt II equals the second parameter $^{234}U/^{238}U$ AR to calculate the $^{230}Th/U$ age.

Osmond et al. (1970) used for their plots I and II the $^{230}Th/^{238}U$ and $^{234}U/^{238}U$ ARs as numerators, respectively, and the $^{232}Th/^{238}U$ AR as common denominator. Both Osmond plots are most sensitive to check the binary mixing concept. One reason is that uranium is easily dissoluble and the corresponding activity ratios react very sensitive to open system conditions with respect to uranium. Thorium is considered as insoluble. Closed-system conditions without gain or loss of both uranium and thorium were checked individually and rigorously for each sample by means of the isotope-ratio evolution plot, and the Rosholt and Osmond plots.

The $^{230}Th/U$ ages (Table 1) were calculated with the half lives of 245.25 and 75.69 ka for ^{234}U and ^{230}Th, respectively (Chen et al., 2000), and are given with 2σ-confidence intervals. To determine the oldest datable $^{230}Th/U$ age of a sample, we assumed that the error ellipse of the uranium and thorium activity ratios (ARs) at the detection limit (defined by the 2-σ confidence interval) touches the isochron of infinite age (Geyh, 2008) in the isotope-ratio evolution plot (Fig. 5). The oldest datable $^{230}Th/U$ ages are unusually old (up to 700 ka) as a result of the very large uranium concentration of most samples.

Pollen analyses were carried out on 1 kg material of the core KOO 928 grown during MIS 11. Decomposed non-identifiable organic matter rather than pollen were found. Reasons may be that pollen were decomposed due to the high humidity in the hot voids, the sediment cover in the catchment of the cave prevented the infiltration of pollen or they were flushed towards the bottom due to the horizontal growth of the stalagmite.

Paleomagnetic measurements of core KOO 930 were conducted. As no paleomagnetic reversal was found the stalagmite formed after the Brunhes–Matuyama geomagnetic reversal at ~780 ka.

Results

Flowstone core

The results of the uranium and thorium activity measurements and the $^{230}Th/U$ age determinations of the flowstone core KOO 933 (Fig. 4) are compiled in Table 1. The ARs of ^{234}U, ^{238}U, ^{230}Th and ^{232}Th of the flowstone core were checked for open systems with respect to uranium as described above. The parameter f (present-day initial $^{230}Th^{+}/^{232}Th$ AR of the detritus thorium) used for the correction of $^{230}Th/U$ dates was taken from the Rosholt I plot. The ARs of uranium and thorium of the flowstone samples fit to straight lines within their confidence intervals (Eq. (1)) in the four Osmond and Rosholt plots and to the isochrons of 400 ka, 230 ka, 200 ka and 120 ka in the isotope-ratio evolution plot (Fig. 5). By this they confirm both the suitability of these samples for $^{230}Th/U$ age determination and the binary mixing concept of radiogenic $^{230}Th^{*}$and detrital $^{230}Th^{+}$. Two outliers F11 and F05 (Table 1; Fig. 5) were identified.

Three flowstone samples (F01, F02, F03) from the 0.8 cm (up to 2.0 cm) thick banded surface layer yielded a mean corrected $^{230}Th/U$ age of 118 ± 2 ka ($\chi^2 = 0.5$) with f = 0.134 ± 0.045. The mean initial $^{234}U/^{238}U$ AR equals 1.2222 ± 0.0170 (present-day mean = 1.1591 ± 0.0016; $\chi^2 = 9.8$). The sampled layer grew during the last warm interglacial MIS 5e (Marine Oxygen Isotope Stage 5e, 130–115 ka). Assuming a maximum growth period of 10 ka during MIS 5e, the deposition rate was between 0.08 and 0.2 mm per century.

Beneath the MIS 5e layers, six flowstone samples from the about 7.5 cm-thick compact core section with differently sized voids formed during the preceding interglacial period (MIS 7, 245–190 ka). The upper three samples (F04, F06, F07) yielded a detritus-corrected mean $^{230}Th/U$ age of 207 ± 2 ka (f = 0.878 ± 0.177; $\chi^2 = 3.2$) and a mean initial $^{234}U/^{238}U$ AR = 1.2011 ± 0.0009 (present-day mean = 1.1194 ± 0.0008; $\chi^2 = 151!$). Sample F05 from this part of the core behaved as a disturbed isotopic U/Th system. The three flowstone samples (F08–F10) from the lowermost part of this core section provided a mean detritus-corrected $^{230}Th/U$ age of 229 ± 2 ka (f = 0.963 ± 0.017; $\chi^2 = 6.0$), corresponding to the oldest part of MIS 7 of the SPECMAP timescale (Imbrie et al., 1984; Lisiecki and Raymo, 2005). The large χ^2 value of 6.0 may be explained by dating of different old samples of this interglacial. The mean initial $^{234}U/^{238}U$ AR is 1.2730 ± 0012 (present-day mean = 1.1428 ± 0.0011; $\chi^2 = 137!$). The deposition rate is around ≥0.14 mm per century.

Below this section, a 5-cm-thick, very porous and sandy layer with iron incrustations may indicate dissolution of carbonate associated with leaching of uranium. The low uranium concentration of the samples F10 and F11 supports this assumption. The mineral content consists mainly of sand especially in the middle part of the flowstone (Fig. 4).

Two flowstone samples (F12, F13) from the 12-cm-thick base layer provided a mean $^{230}Th/U$ age of 386 ± 6 ka ($\chi^2 = 2.7$) and a mean initial $^{234}U/^{238}U$ AR of 1.0727 ± 0.0018 (present-day mean = 1.0244 ± 0.0017; $\chi^2 = 4$), thus confirming speleothem growth during the pre-penultimate interglacial MIS 11 (420–385/360 ka; discrepant estimates of the length of MIS 11). Assuming a calcareous sinter growth period of about 35 ka, the minimum deposition rate was ≥0.35 mm/100 yr; some of the sinter might have been eroded. The sample F11 (Fig. 5) deposited in this period behaved as a disturbed isotopic U/Th system.

The $^{230}Th/U$ ages of the flowstone provided evidence that secondary carbonate was only deposited during the pronounced interglacial periods of MIS 11, MIS 7 and MIS 5e rather than during the glacial periods MIS 10, MIS 8 and MIS 6. There are indications that carbonate was dissolved during MIS 9. The uranium concentration of the flowstone fluctuated widely between 1370 and 5340 ppb.

Stalagmite cores

Most $^{230}Th/^{232}Th$ ARs of the stalagmite cores (KOO 929–931) were >50 excluding substantial contamination with detrital $^{230}Th^{+}$. Then, $^{230}Th/U$ ages with and without correction for detrital $^{230}Th^{+}$ do not differ (Table 1). The relationship between uranium concentration and depth within the cores KOO 929–931 reflects some degree of uranium mobilization especially within the middle part of the stalagmite. Many activity ratios deviate from straight lines in both Osmond plots (Fig. 6), providing evidence for disturbed isotopic uranium series systems (M01, M03, M04, M06, M08, M10, M12, M13, M14, M15a, M17, M17a, M18, M23–M27). All other data in Table 1 were suitable for $^{230}Th/U$ dating.

Several adjacent sample pairs (less than a few centimeters distant from each other) M07/M08, M12/M13, M15/M16, M17/M17a, and M21/M22 from the middle core of the stalagmite had both depleted and enriched uranium concentrations. The most enriched samples M08 and M18 contained 10,120 and 9730 ppb U which is more than twice the concentration of the rim layer (4060 ppb). Several of the samples were not datable or showed jumps in their $^{230}Th/U$ ages (Table 2).

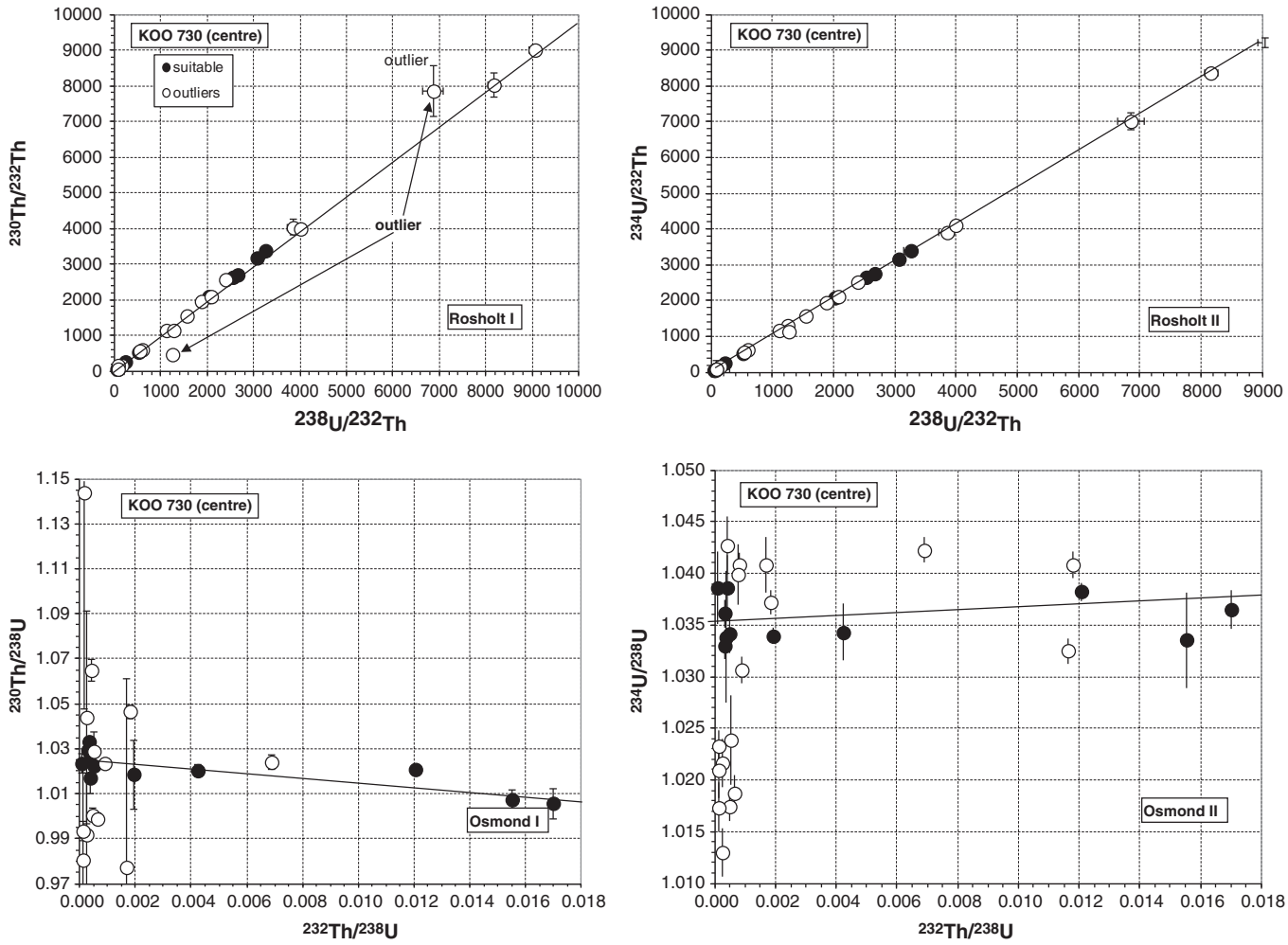

Figure 6. Rosholt (1976) and Osmond et al. (1970) plots of the data obtained from middle core KOO 930 for the check of closed-system conditions of uranium. The Rosholt I plot shows two outliers (open symbols) while the Osmond I and Osmond II plots show many outliers taking into account the requirement of linear relationships. The activity ratios of dots distant from straight lines were not suitable for reliable ^{230}Th/U dating. Suitable data using for ^{230}Th/U dating are shown as filled black symbols.

Three samples from the upper core (U01, U03, U04) yielded a mean ^{230}Th/U age of 382 ± 5 ka ($\chi^2 = 4.7$) and an initial ^{234}U/^{238}U AR = 1.1102 ± 0.0012 (present-day mean = 1.0374 ± 0.0011; χ^2 = 16). The ample U02 behaved as disturbed isotopic U/Th system.

The samples from the middle core (M02, M05, M07, M09, M11, M15, M16, M19, M20, M21, M22) have a mean ^{230}Th/U age of 392 ± 4 ka and an initial ^{234}U/^{238}U AR of 1.0991 ± 0.0005 (present-day mean = 1.0327 ± 0.0005; $\chi^2 = 232$).

Two ^{230}Th/U ages of the lower core (L01, L02) yielded ^{230}Th/U ages of 369 ± 8 and 439 ± 18 ka (mean 381 ± 7 ka; $\chi^2 = 13$! Due to the large χ^2 the mean ^{230}Th/U age may not be meaningful) and an initial ^{234}U/^{238}U AR of was 1.1419 ± 0.0019 (present-day mean = 1.0483 ± 0.0017; $\chi^2 = 8$). Both ^{230}Th/U ages provided evidence that secondary carbonate was deposited at least during a long interval of MIS 11. The sample L03 behaved as disturbed isotopic U/Th system.

Table 2
Jumps of the uranium concentration and ^{230}Th/U ages of adjacent samples (OS = open system with respect to uranium).

Sample	M07/M08	M12/M13	M15/M16	M17/M18	M21/M22
Depth (cm)	11.4/12.7	15.3/16.0	19.2/21.3	21.3/22.6	25.8/27.7
^{230}Th/U age (ka)	360/~90	440/> OS	410/480	>OS/>400	390/347
U conc. (ppm)	4.8/10.1	4.3/2.3	4.5/2.9	3.1/9.7	8.8/4.4

The isotope-ratio evolution plot (Fig. 7) shows initial ^{234}U/^{238}U AR evolution lines of 1.05, 1.10, 1.15, and 1.20 as well as straight "isochrons" of 550 ka, 450 ka, and 350 ka. The ARs of L03, M04, M10, M13, M17 and M17a plot far right to the isochron of infinite age and yield oldest datable ^{230}Th/U ages. The sample M1.1 from the visible rim side yielded a ^{230}Th/U age of 121 ± 3 ka and had a slightly larger initial ^{234}U/^{238}U AR of 1.13. The layer formed during MIS 5e.

In summary, closed-system conditions with respect to uranium existed for most rim samples while many samples from the middle part of the stalagmite behaved as open systems with respect to uranium.

Interpretation

Based on the presented ^{230}Th/U dates, the continuous growth of the stalagmite in the Rössing Cave (Fig. 9) started 420 ka ago (onset of MIS 11) and lasted until the termination of MIS 11 at around 385 ka (Geyh and Müller, 2005) or even later at 360 ka (Chen et al., 2002, Roberts et al., 2012). MIS 11 was an unusually warm and long-lasting interglacial period (Howard, 1997; Droxler and Farrell, 2000; Brook, 2005). Adopting a duration of 35 ka or possibly 60 ka the deposition rate was around 2.6 or 1.5 mm/100 yr, respectively, of the 90 cm high stalagmite or one order of magnitude larger than that of the flowstone. Both rates can be compared with each other as the areal extension of the stalagmite and of the flowstone are similar large.

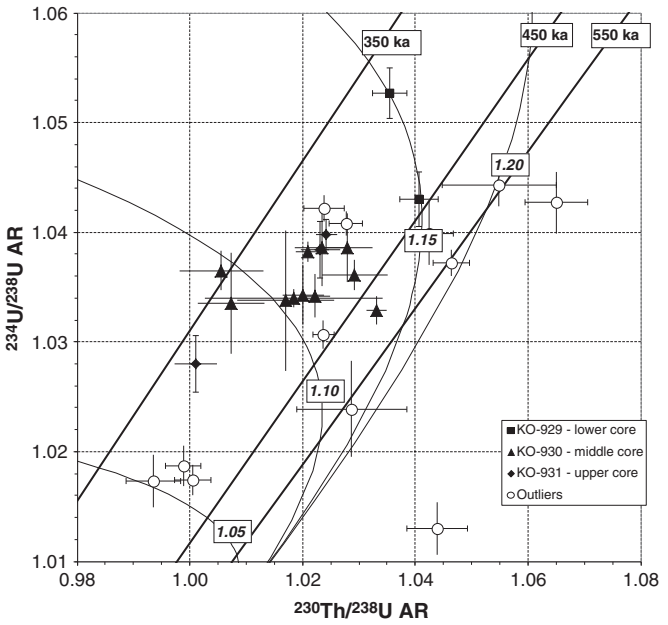

Figure 7. Isotope-ratio evolution plot of the $^{234}U/^{238}U$ AR versus the $^{230}Th/^{238}U$ AR (Kaufman and Broecker, 1965) of the stalagmite cores (KOO 929–931) used as check for closed-system conditions with respect to uranium. The evolution curves of the initial $^{234}U/^{238}U$ AR 1.05, 1.10, 1.15, and 1.20 as well as the "isochrons" of 350, 450, and 550 ka are shown. The outlier data (data in italics in Table 1; open symbols) were identified by both Osmond I and II plots (Fig. 6). They belong to samples with identified uranium mobilization. The data suitable for $^{230}Th/U$ dating (filled symbols) scatter between the "isochrons" of 450 and 350 ka.

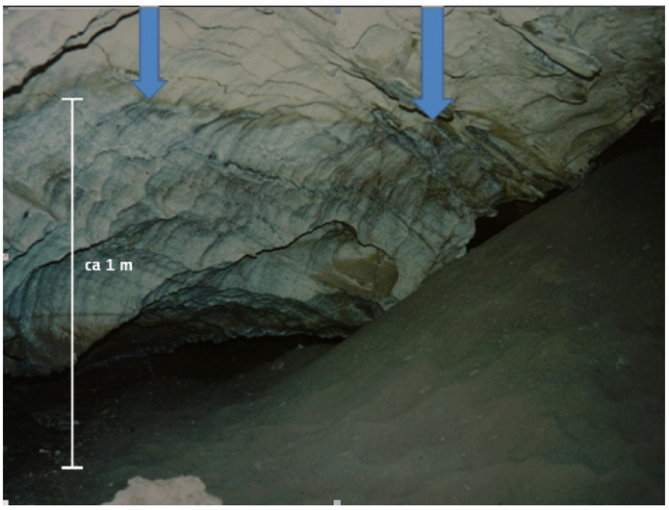

Figure 8. The lower part of the cave wall up to 1 m looked dirtier than the upper part. The arrows mark the proposed inundation at MIS 9. Eolian sand forms the slope on the right side of the photograph.

The diameter of the stalagmite (Fig. 2) shrinks just above the position of the middle core from 60 cm to 40 cm. This might be due to a lowering of the rate of drip-water flow after the first half of its growth during MIS 11, because this parameter controls the diameter of an ideally grown stalagmite. The deposition rate of stalagmites depends on the HCO_3 concentration of the drip water (Dreybroth and Franke, 1987). Once the stalagmite approached the roof of the cave, the surface of the stalagmite and of the flowstone were covered with a thin and bright colored carbonate layer.

Furrows and grooves in the outermost layer of the stalagmite and the bent growth lines (Fig. 3) may be considered as indication that the percolating drip water might have dissolved uranium (preferentially ^{234}U) and re-deposited somewhere in voids of deeper lying parts of the stalagmite. In addition, any subsequent penetration of humidity might also have caused post-depositional uranium mobilization. Loss and gain of ^{234}U explain underestimated, overestimated or missing (open system) $^{230}Th/U$ ages (as oldest datable $^{230}Th/U$ ages), respectively. Most of the inner part of the stalagmite might have been affected by these processes.

There is only very limited information on the deposition of secondary carbonate in the Rössing Cave during MIS 9 (ca. 300 ka). The very porous, sandy and mechanically unstable section of the flowstone between the MIS 11 and MIS 7 layers (Fig. 4) contained iron incrustations and might have been formed during this period. These distinctive features of this core section have to be related to a wet period in the Namib Desert. A missing sediment cover above the cave might have prevented an enrichment of CO_2 in the drip water and by this a deposition of secondary calcite. The generated acidic water dissolved carbonates and allowed forming iron incrustations. The ≤1-m-high less dirty lower part of the cave walls may be caused by inundations during MIS 9 (Fig. 8), which would have reached the top of the stalagmite. Based on OSL dates of >90 ka and >65 ka of blown-in sand deposits floodwaters if any can have inundated the cave only before 90 ka. However, no final conclusion was reached about what really happened in the Namib Desert during MIS 9.

A compact flowstone (F04–F07 and F08–F10: mean $^{230}Th/U$ ages of 207 ± 2 ka and 229 ± 2 ka, respectively) as well as a thin banded surface on the stalagmite (M1.2: $^{230}Th/U$ age of 213 ± 9 ka) deposited during MIS 7. Some iron incrustations formed only at the beginning. Scarce evidence for a wetter climate is provided by $^{230}Th/^{234}U$ dates between 240 and 210 ka of lake-bed carbonates from Narabeb, ca. 170 km south of the Rössing Cave in the Namib dune field (Selby et al., 1979).

During MIS 5 a compact sinter formed on both the flowstone (F01–F03: mean $^{230}Th/U$ age of 118 ± 2 ka) and the surface of the stalagmite (M1.1: $^{230}Th/U$ age of 121 ± 3 ka) during a wet period also documented by OSL dates in the range from 128 ka to 75 ka of water-lain interdune deposits in the northern Namib Sand Sea (Stone et al., 2010a,b). Hydrologic excursions with lake high-stands between 110 ka and 89 ka are likewise known in the Kalahari (Stone et al., 2010b).

The presented $^{230}Th/U$ ages >100 ka of material with ^{14}C dates between 41 and 27 ^{14}C ka BP (Heine and Geyh, 1984) do not longer support the postulated pluvial period in the Namib Desert. Similar results are published from the Tinkas Caves with $^{230}Th/^{234}U$ ages >220 ka and ^{14}C ages between 49 and 34 ^{14}C ka BP (Heine, 1991). All these samples collected from surface layers of speleothems were obviously slightly contaminated with traces of a few percent of young sinter and therefore yielded apparently underestimated ^{14}C ages.

For the first time, our $^{230}Th/U$ dates from the Rössing Cave provided reliable proxy data for a continuous wet climate record in MIS 11, MIS 9, MIS 7 and MIS 5, at least for the region around the Rössing Cave in the central Namib Desert. The precision of the $^{230}Th/U$ dates, however, is not sufficient to decide whether the deposition of secondary carbonates was continuous or intermittent during these interglacial periods. There is a trend of decreasing sinter formation from MIS 11 to the later interglacials. The deposition rate of the flowstone decreased from >2.6 to <0.35 mm per century.

The growth periods of speleothem in the Central Namib correlate well with Pleistocene wet periods of the Sahara-Arabian arid belt of the northern hemisphere (Fig. 9). Numerically dated lacustrine sediments from eastern Sahara provide for the first time evidence for both, a distinct grouping of the $^{230}Th/U$ ages in the stages MIS 9, 7 and 5 and a decreasing intensity of the pluvial episodes towards the present

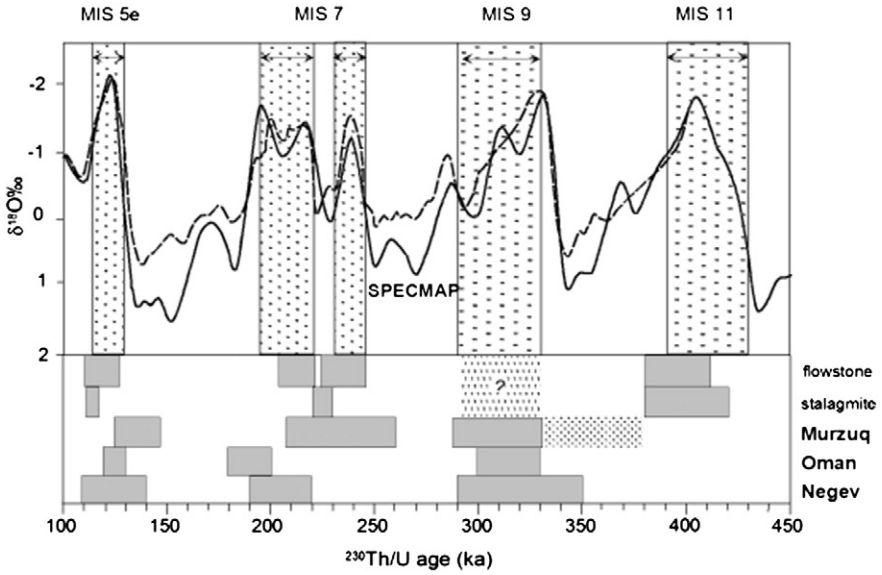

Figure 9. At least three but probably four growth periods of the stalagmite and of the flowstone in the Rössing Cave represent first evidence of middle Pleistocene wet periods in the central Namib Desert of the southern hemisphere. They correlate well with the $\delta^{18}O$ curves of SPECMAP (Imbrie et al., 1984; Lisiecki and Raymo, 2005) and coincide with periods of tufa formation in the Murzuq Basin, Libyan Sahara (Szabo et al., 1995; Thiedig et al., 2000; Geyh and Thiedig, 2008), the growth of speleothems in the Hoti Cave in Oman (Fleitmann et al., 2003; Fleitmann and Matter, 2009), and in caves of the Negev Desert, Israel (Vaks et al., 2010).

(Szabo et al., 1995). These results are confirmed by ^{230}Th/U dates of tufa from the Murzuq Basin (Thiedig et al., 2000; Geyh and Thiedig, 2008) which provide evidence for three pluvials in the present hyper-arid region of North Africa. The deposition periods lasted from 380 to 290 ka, 260 to 205 ka and 140 to 125 ka with decreasing intensity. The pluvial coinciding with MIS 9 in the Murzuq Basin appears to be prolongated as the ^{230}Th/U dates are obtained from breccias with material from the preceding interglacial. The ^{230}Th/U dates of speleothem samples from caves of the hyper-arid Kharga Oasis in Egypt confirm calcareous sinter formation in MIS 7 and MIS 5e (Brook et al., 2003).

Speleothem formation in many caves in the Negev Desert, Israel, occurred at 350–290 ka, 220–190 ka and 142–109 ka (Vaks et al., 2010). Based on reliable OSL dates of quartz extracts of lake deposits in the Nafud desert, Saudi Arabia (Rosenberg et al., 2013), applying the SAR protocol for thermally transferred optically stimulated luminescence (TT-OSL) provides evidence of wet climate approximately ca. 410 ka, 320 ka, 200 ka, 125 ka, and 100 ka. Samples from the same sites yielded underestimated ^{14}C ages between 40 and 20 ^{14}C ka BP. Speleothems from the Hoti Cave in northern Oman document wet conditions at 330–300 ka, 200–180 ka and 130–120 ka, in addition to around 80 ka and at 10–6 ka (Burns et al., 2001; Fleitmann et al., 2003; Fleitmann and Matter, 2009). In northern Oman, present precipitation amounts to about 40 mm/yr.

The strong coincidence of wet periods in the mentioned arid regions in the northern and southern hemispheres with the interglacials MIS 11, 9, 7, and 5 is striking and supports an interhemispheric synchrony of major climatic events. This holds also true for the trend of increasing aridity of the interglacial periods since the middle Pleistocene. The missing Holocene carbonate formation in all hyper-arid regions except for minor sinter formation in Oman and southern Saudi Arabia is its most pronounced peculiarity. In arid North Africa is a trend of decreasing precipitation from MIS 11 to MIS 5e derived from the intensity of tufa formation (Szabo et al., 1995; Thiedig et al., 2000; Geyh and Thiedig, 2008). Rosenberg et al. (2013) report that a single, perennial lake covering the entire southwestern Nafud in Saudi Arabia ca 320 ka ago was much smaller and restricted to interdune depressions of a pre-existing dune relief at 200 ka, 125 ka, and 100 ka. Holocene lake deposits were not identified.

An estimate on the quantity of drip water explaining the growth rate of the stalagmite and the flowstone in the Rössing Cave allows a better definition of the used term “wet paleoclimate.” The formation of secondary carbonate requires drip water with an excess of dissolved CO_2 entering into the cave. Seeping rainwater usually acquires its high CO_2 concentration in the top soil to a level of up to 100× higher than that of the atmospheric air. In soil, plants and lichen respire as well as fungi and omnipresent bacteria decompose organic matter producing CO_2. Hence, during the limited periods of speleothem formation a thin soil and/or a thin vegetated sediment layer must have covered the cave. The occurrence of intermittent periods of surface burial by sediments or desert soils on which arid-adapted vegetation developed at least in the catchment of the cave is neither challenged by either the surface exposure ages of over a million years (Bierman and Caffee, 2001; Van der Wateren and Dunai, 2001) nor the formation of gypcrete soils (Heine and Walter, 1996). The sediment cover proposed for the formation of speleothems existed maximum several 10 ka and was most probably restricted to small parts of the desert while the exposure ages confirm desert conditions for a period of at least two orders of magnitude longer.

With a mean diameter of 45 cm of the Rössing Cave stalagmite and a maximum growth rate of 2.5 mm per century a carbonate deposition rate of 16 cm^3/yr ≈ 32 g/yr or 0.32 mol C/yr is required. This corresponds to 80 l/yr of drip water with a bicarbonate concentration of minimum 4 mmol C/l. Adapting an evapotranspiration rate of up to 99% for rain und 100% for fog, 8000 l of rainwater is required forming drip water.

This quantity was easily gathered on an area of only 16,000 m^2 (circle with a diameter of 70 m) at a precipitation rate of 50 mm/yr (present average rainfall is 5–18 mm/yr). As the marble ridge merges the surface runoff from the descending plain east of the cave (Fig. 1), a catchment area of a few km^2 was sufficient for the growth of the stalagmite, even if the rate of the annual precipitation or/and the bicarbonate concentration in the drip water were considerably lower. These figures illustrate that intensive humid or pluvial periods had not been necessary for the formation of the speleothems in the Rössing Cave.

The results of this estimate and the requirement of at least a thin vegetated sediment cover within the restricted catchment of the

cave system allow now to specify the used term "wet period." Nevertheless, the central Namib Desert shows spots with a great variety of plants—lichens mainly on gypsum plains, grass with some bushes and trees on the calcrete plains, large trees in the dry valleys (Seely and Pallett, 2008; Schachtschneider and February, 2010)—that are adapted to the harsh climatic conditions. However, more frequent interglacial rainfall events in an arid climate, compared to the glacial periods, as expected from our study should have caused a denser plant cover on the calcrete and gypsum plains in the central Namib Desert. Hence, the terms "humid" or even stronger "pluvial" periods were not considered as adequate. Apparently, the 'wet periods' recorded in the Rössing Cave speleothems indicate an expanded summer rainbelt with monsoonal precipitation originating from the Indian Ocean. Applying the Köppen–Geiger system of climate classification (Strahler, 1960), the dry climate (BW) was dominant. During the interglacials MIS 11, MIS 9, MIS 7 and MIS 5 the dry climate with wet phases changed towards BS (foggy coastal steppes).

The terrestrial fraction of marine sediments from the Atlantic Ocean off Namibia used to reconstruct the climate in the Namib Desert yielded ambiguous results. In accordance with our finding, Collins (2011) and Collins et al. (2011, 2013) postulated a wetter interglacial climate than that of the glacial periods in the central Namib Desert. They concluded that the tropical African summer rain belt contracted during glacials and expanded during interglacials.

In contrast, Stuut et al. (2002) and Stuut and Lamy (2004) based their climatic conception on a statistical treatment of grain-size distributions of the terrestrial fraction in marine sediments. Two of the identified end members were interpreted as coarse eolian dust and the third as hemipelagic mud. The ratio of the two eolian end members was assumed to be controlled by the intensity of the SE trade winds, which are assumed to be more intensive during glacials than interglacial periods. Hence, these authors postulated an increased aridity during interglacial periods (Stuut et al., 2002). This finding may not conflict with our conclusion that the interglacial periods experienced a wetter climate than the glacial periods. There might have been still large areas without sediment cover during the interglacial periods to deliver sufficient dust for the marine sediments though the modeled climate/sediment interpretation might have to be revised.

It is not the task of this paper to explain discrepant climatic concepts on the climate of the Namib Desert derived from marine sediment studies. Many authors (e.g., Little et al., 1997; Stuut et al., 2002, 2011; Pichevin et al., 2005; Gasse et al., 2008; Collins, 2011) already thoroughly discussed the difficulty of reconstructing paleoclimates from marine sediments due to the poor understanding of the fluvial and eolian transport processes of terrestrial material to the oceans (Lee-Thorp and Schneider, 2002; Heine and Völkel, 2010).

One topic is left for the interpretation. The range of $^{234}U/^{238}U$ ARs for each formation period was always much larger than expected from the analytical precision. This finding did not seriously affect the $^{230}Th/U$ dates. Calculations with the minimum and maximum $^{234}U/^{238}U$ ARs of each formation period resulted in a shift of ≤ 8 ka. However, the $^{234}U/^{238}U$ ARs yield some information on the source of the dissolved uranium in the drip water.

There are two sources: The $^{234}U/^{238}U$ ARs of the samples from the middle core (KOO 930) formed in MIS 11 and MIS 9 were slightly larger towards the visible side (>1.029) than towards the wall side (M23–M27: <1.023). Obviously the drip water on the wall side contained less ^{234}U than that on the front side. In contrast, the flowstone formed since MIS 7 (F01–F10) and the rim layer of the stalagmite deposited in MIS 5e (M1.1) had a higher value (>1.10–1.18). This change of the $^{234}U/^{238}U$ AR indicated that during the first phase of the stalagmite growth in MIS 11 and MIS 9 drip water dissolved only weathered limestone from which much easily soluble excess ^{234}U due was leached. Since MIS 7, drip water also dissolved uranium from secondary carbonates formed in the cave resulting in increased $^{234}U/^{238}U$ ARs (Wakshal and Yaron, 1974).

Conclusion

The long 420-ka $^{230}Th/U$ record from speleothems of the Rössing Cave provided for the first time a continuous chronology on the paleoprecipitation in the central Namib Desert and possibly other arid areas of southern Africa. It also settles the debate on the interhemispheric synchrony of interglacial pluvial periods in deserts for the last four interglacial/glacial cycles. Moreover, these results may help to refine the ambiguous climatic interpretation of marine records off southwestern Africa. The $^{230}Th/U$ dates of speleothems in the Rössing Cave provide evidence that several wet periods interrupted the dominant hyper-arid climate in the Namib Desert during the last 420 ka. These wet periods coincided with the warm interglacials of the 100-ka-Milankovitch cycles of the orbital forcing of the global temperature (Imbrie et al., 1984) (Fig. 9), with warmer SSTs and with a reduced dust input (Jahn et al., 2003) in the Benguela Current. These wet periods resulted from an at least weakly increased precipitation compared to the present. The intensity of these wet periods became weakened from M 11 to the present. MIS 1 (Holocene) does not show speleothem formation.

Acknowledgments

We acknowledge the performance of chemical analyses and mass spectrometric measurements by Deniz Özen, Gudrun Drewes and Sabine Mogwitz, Leibniz Institute of Geophysical Research, Hannover. Louis Scott, Bloemfontein, kindly searched for pollen. Ludwig Zöller, Bayreuth, determined TL ages of the cave deposits and Frank Sirocko, Mainz, made paleomagnetic measurements. Rolf Walter, Germany, provided detailed information on the geologic setting of the Rössing Cave and the identification of rocks. Michael Roberts, Vancouver, improved the English language and gave critical comments. The manuscript substantially gained by the critical reading and suggestions of the reviewers David Fink, AE QR, Alan R. Gillespie, E QR, and John S. Compton, Cape Town, South Africa. The German Research Foundation financed the sampling in the Rössing Cave (DFG He 722/14-5).

References

Besler, H., Blümel, W.-D., Heine, K., Hüser, K., Leser, H., Rust, U., 1994. Geomorphogenese und Paläoklima Namibias. Eine Problemskizze. Erde 125, 139–165.
Bierman, P., Caffee, M., 2001. Slow rates of rock surface erosion and sediment production across the Namib Desert and escarpment, Southern Africa. American Journal of Science 301, 326–358.
Bischoff, J.L., Fitzpatrick, J.A., 1991. U-series dating of impure carbonates: an isochron technique using total-sample dissolution. Geochimica et Cosmochimica Acta 55, 543–554.
Brook, E.J., 2005. Atmospheric Science: Tiny Bubbles Tell All. Science 310, 1285–1287.
Brook, G.A., Cowart, J.B., Marais, E., 1996. Wet and dry periods in the southern African summer rainfall zone during the last 300 kyr from speleothem, tufa and sand dune age data. Palaeoecology of Africa 24, 147–158.
Brook, G.A., Embabi, N.S., Ashour, M.M., Edwards, R.L., Cheng, H., Cowart, J.B., Dabous, A.A., 2003. Quaternary environmental change in the Western Desert of Egypt: evidence from cave speleothems, spring tufas, and playa sediments. Zeitschrift für Geomorphologie N.F., Supplement 131, 59–87.
Burns, S.J., Fleitmann, D., Matter, A., Neff, U., Mangini, A., 2001. Speleothem evidence from Oman for continental pluvial events during interglacial periods. Geology 29, 623–625.
Chen, H., Edwards, R.L., Hoff, J., Gallup, C.D., Richards, D.A., Asmeron, Y., 2000. The half-lives of uranium-234 and thorium-230. Chemical Geology 169 (1–2), 17–33.
Chen, M.-T., Chang, Yuan-Pin, Chang, Cheng-Chieh, Wang, Li-Wen, Wang, Chung-Ho, Ein-Fen, Yu., 2002. Late Quaternary sea-surface temperature variations in the southeast Atlantic: a planktic foraminifer faunal record of the past 600 000 yr (IMAGES II MD962085). Marine Geology 180, 163–181.
Collins, J.A., July 2011. Glacial to Holocene Hydroclimate In Western Africa: Insights from Organic and Major Element Geochemistry of Hemipelagic Atlantic Ocean Sediments. PhD Thesis Faculty of Geosciences at the University of Bremen (108 pp.).
Collins, J.A., Schefuß, E., Heslop, D., Mulitza, S., Prange, M., Zabel, M., Tjallingii, R., Dokken, T.M., Huang, E., Mackensen, A., Schulz, M., Tian, J., Zarriess, M., Wefer, G., 2011. Interhemispheric symmetry of the tropical African rain belt over the past 23,000 years. Nature Geoscience 4, 42–45.
Collins, J.A., Schefuß, E., Mulitza, S., Prange, M., Werner, M., Tharammal, T., Paul, A., Wefer, G., 2013. Estimating the hydrogen isotopic composition of past precipitation using leaf-waxes from western Africa. Quaternary Science Reviews 65, 88–101.

Dreybroth, W., Franke, H.W., 1987. Wachstumsgeschwindigkeiten und Durchmesser von Kerzenstalagmiten. Höhle 38 (1), 1–6.

Droxler, A.W., Farrell, J.W., 2000. Marine Isotope Stage 11 (MIS 11): new insights for a warm future. Global Planetary Change 24, 1–5.

Eckardt, F.D., Soderberg, K., Coop, L.J., Muller, A.A., Vickery, K.J., Grandin, R.D., Jack, C., Kapalanga, T.S., Henschel, J., 2013. The nature of moisture at Gobabeb, in the central Namib Desert. Journal of Arid Environment 93, 7–19.

Fleitmann, D., Matter, A., 2009. The speleothem record of climate variability in southern Arabia. Comptes Rendus Geosciences 341, 633–642.

Fleitmann, D., Burns, S.J., Neff, U., Mangini, A., Matter, A., 2003. Changing moisture sources over the last 330,000 years in northern Oman from fluid-inclusion evidence in speleothems. Quaternary Research 60, 223–232.

Gasse, F., Chalié, F., Vincens, A., Williams, M.A.J., Williamson, D., 2008. Climatic patterns in equatorial and southern Africa from 30,000 to 10,000 years ago reconstructed from terrestrial and near-shore proxy data. Quaternary Science Reviews 27, 2316–2340.

Geyh, M.A., 2008. Selection of suitable data sets improves ^{230}Th/U dates of dirty material. Geochronometria 30, 69–77. http://dx.doi.org/10.2478/v10003-008-0001-1.

Geyh, M.A., Franke, H.W., 1970. Zur Wachstumsgeschwindigkeit von Stalagmiten. Atompraxis 16, 1–3.

Geyh, M.A., Müller, H., 2005. Numerical ^{230}Th/U dating and a palynological review of the Holsteinian/Hoxnian Interglacial. Quaternary Science Review 24, 1861–1872.

Geyh, M.A., Thiedig, F., 2008. The Middle Pleistocene Al Mahrúqah Formation in the Murzuq Basin, northern Sahara, Libya evidence for orbitally-forced humid episodes during the last 500,000 years. Palaeogeography, Palaeoclimatolology, Palaeoecolology 257, 1–21.

Heine, K., 1991. Paläoklima und Reliefentwicklung der Namibwüste im überregionalen Vergleich. Geomethodica 16, 53–92.

Heine, K., 1992. On the ages of humid Late Quaternary phases in southern African arid areas (Namibia, Botswana). Palaeoecolology of Africa 23, 149–164.

Heine, K., 1998. Climatic change over the past 135,000 years in the Namib Desert (Namibia) derived from proxy data. Palaeoecology of Africa 25, 171–198.

Heine, K., Geyh, M.A., 1984. Radiocarbon dating of speleothem from the Rössing cave, Namib desert, and palaeoclimatic implications. In: Vogel, J.C. (Ed.), Late Cainozoic Palaeoclimates of the Southern Hemisphere. Balkema, Rotterdam, pp. 465–470.

Heine, K., Völkel, J., 2010. Soil clay minerals in Namibia and their significance for the terrestrial and marine past global change research. African Study Monographs Supplements Issue 40, 31–50.

Heine, K., Walter, R., 1996. Gypcretes of the central Namib Desert (Namibia). Palaeoecology of Africa 24, 173–201.

Howard, W., 1997. A warm future in the past. Nature 388, 418–419.

Imbrie, J., Hays, J.D., Martinson, D.G., McIntyre, A., Mix, A.C., Morley, J.J., Pisias, N.G., Prell, W.L., Shackleton, N.J., 1984. The orbital theory of Pleistocene climate: support from a revised chronology of the marine ^{18}O record. In: Berger, A.L., Imbrie, J., Hays, J., Kukla, G. (Eds.), Milankovitch and Climate. Reidel, Dordrecht, pp. 269–305.

Ivanovich, M., Harmon, R.S. (Eds.), 1992. Uranium Series Disequilibrium: Applications to Earth, Marine and Environmental Sciences. Clarendon Press, Oxford (920 pp.).

Jahn, B., Donner, B., Müller, P.J., Röhl, U., Schneider, R.R., Wefer, G., 2003. Pleistocene variations in dust input and marine productivity in the northern Benguela Current: evidence of evolution of global glacial–interglacial cycles. Palaeogeography, Palaeoclimatology, Palaeoecology 193, 515–533.

Kaufman, A., 1993. An evaluation of several methods for determining 230Th/U ages in impure carbonates. Geochimica et Cosmochimica Acta 57, 2303–2317.

Kaufman, A., Broecker, W., 1965. Comparison of ^{230}Th and ^{14}C ages for carbonate materials from lakes Lahontan and Bonneville. Journal of Geophysical Research 70 (16), 4039–4054.

Ku, T.L., Liang, Z.Ch., 1984. The dating of impure carbonates with decay-series isotopes. Nuclear Instrumuments and Methods in the Physical Research 223, 563–571.

Lancaster, J., Lancaster, N., Seely, M.K., 1984. Climate of the central Namib Desert. Madoqua 14 (7), 769–782.

Lee-Thorp, J., Schneider, R., 2002. Linking the continental environmental Quaternary history of southern Africa with ocean currents and Antarctica. PAGES News 10 (2), 2.

Lisiecki, L.E., Raymo, M.E., 2005. A Pliocene–Pleistocene stack of 57 globally distributed benthic δ^{18}O records. Paleoceanography 20, PA1003. http://dx.doi.org/10.1029/2004PA001071.

Little, M.G., Schneider, R.R., Kroon, D., Price, B., Summerayes, C.P., Segal, M., 1997. Tradewind forcing of upwelling, seasonality, and Heinrich events as a response to sub-Milankovitch climate variability. Paleooceanography 12, 568–576.

Mendelsohn, J., Jarvis, A., Roberts, C., Robertson, T., 2002. Atlas of Namibia. A Portrait of the Land and Its People.Philip Publ, Cape Town (200 pp.).

Ollier, C.D., 1977. Outline geological and geomorphic history of the central Namib Desert. Madoqua 10 (3), 207–212.

Osmond, J.K., May, J.P., Tanner, W.F., 1970. Age of the Cape Kennedy barrier and lagoon complex. Journal of Geophysical Research 75 (2), 469–479.

Partridge, T.C., Maud, R.R., 1987. Geomorphic evolution of Southern Africa since the Mesozoic. South African Journal of Geology 90, 179–208.

Pichevin, L., Cremer, M., Giraudeau, J., Bertrand, P., 2005. A 190 ky record of lithogenic grain-size on the Namibian slope: forging a tight link between past wind-strength and coastal upwelling dynamics. Marine Geology 218, 81–96.

Roberts, D.L., Karkanas, P., Jacobs, Z., Marean, C.W., Roberts, R.G., 2012. Melting ice sheets 400,000 yr ago raised sea level by 13 m: past analogue for future trends. Earth and Planetary Science Letters 357 (358), 226–237.

Rosenberg, T.M., Preusser, F., Risberg, J., Plikk, A., Kadi, K.A., Matter, A., Fleitmann, D., 2013. Middle and Late Pleistocene humid periods recorded in palaeolake deposits of the Nafud desert, Saudi Arabia. Quaternary Science Reviews 70, 109–123.

Rosholt, J.N., 1976. ^{230}Th/U dating of travertine and caliche rinds. Geological Society of America 8, 1076 (Abstracts with Programs).

Schachtschneider, K., February, E.C., 2010. The relationship between fog, floods, groundwater and tree growth along the lower Kuiseb River in the hyperarid Namib. Journal of Arid Environments 74, 1632–1637.

Scholz, D., Hoffmann, D., 2008. ^{230}Th/U-dating of fossil corals and speleothems. E&G: Quaternary Science Journal 57 (1–2), 52–76.

Seely, M., Pallett, J., 2008. Namib. Secrets of a Desert Uncovered. Venture Publications, Windhoek 202.

Selby, M.J., Hendy, C.H., Seely, M.K., 1979. A Late Quaternary lake in the central Namib Desert, southern Africa, and some implications. Palaeogeography, Palaeoclimatology, Palaeoecology 26, 37–41.

Stone, A.E.C., Thomas, D.S.G., Viles, H.A., 2010a. Late Quaternary palaeohydrological changes in the northern Namib Sand Sea: new chronologies using OSL dating of interdigitated aeolian and water-lain interdune deposits. Palaeogeography, Palaeoclimatology, Palaeoecology 288, 35–53.

Stone, A.E.C., Viles, H.A., Thomas, L., van Calsteren, P., 2010b. Quaternary tufa deposition in the Naukluft Mountains, Namibia. Journal of Quaternary Science 25, 1360–1372. http://dx.doi.org/10.1002/jqs.1435 (IP/937/1106) GC.

Strahler, A.N., 1960. Physical Geography.Wiley and Sons, New York — London 534.

Stuut, J.-B.W., Lamy, F., 2004. Climate variability at the southern boundaries of the Namib (southwestern Africa) and Atacama (northern Chile) coastal deserts during the last 120,000 yr. Quaternary Research 62, 301–309.

Stuut, J.-B.W., Maarten, A.P., Schneider, R.R., Weltje, G.J., Jansen, J.H.F., Postma, G., 2002. A 300-kyr record of aridity and wind strength in southwestern Africa: inferences from grain-size distributions of sediments on Walvis Ridge, SE Atlantic. Marine Geology 180, 221–233.

Stuut, J.B.W., Temmesfeld, F., De Deckker, P., 2011. Late Quaternary aridity changes in the winter-rain areas on the southern hemisphere: inferences from the marine sediment archive. ADOM-MARUM Dust Workshop 2011, Abstract, Short Presentations and Posters. 52.

Szabo, B.J., Haynes Jr., C.V., Maxwell, T.A., 1995. Ages of Quaternary pluvial episodes determined by uranium-series and radiocarbon dating of lacustrine deposits of Eastern Sahara. Palaeogeography, Palaeoclimatology, Palaeoecology 113, 227–242.

Thiedig, F., Oezen, D., El-Chair, M., Geyh, M.A., 2000. Evidence of a large Quaternary lacustrine palaeo-lakes in Libya and their importance for climate change in north Africa. In: Sola, M.A., Worsley, D. (Eds.), Proc. Regional Aquifer Systems in Arid Zones — Managing Non-Renewable Resources. Geological Exploration in Murzuq Basin, Chapter 5. Elsevier Science, Amsterdam, pp. 89–116.

Vaks, A., Bar-Matthews, M., Matthews, A., Ayalon, A., Frumkin, A., 2010. Middle-Late Quaternary paleoclimate of northern margins of the Saharan-Arabian Desert: reconstruction from speleothems of Negev Desert, Israel. Quaternary Science Reviews 29, 2647–2662.

Van der Wateren, F.M., Dunai, T.J., 2001. Late Neogene passive margin denudation history — cosmogenic isotope measurements from the central Namib Desert. Global and Planetary Change 30, 271–307.

Vermeesch, P., Fenton, C.R., Kober, F., Wiggs, G.F.S., Bristow, C.S., Xu, S., 2010. Sand residence times of one million years in the Namib Sand Sea from cosmogenic nuclides. Nature Geoscience 3, 862–865.

Wakshal, E., Yaron, F., 1974. ^{234}U/^{238}U disequilibrium in waters of the Judea group (Cenomanian–Turonian) aquifer in Galilee northern Israel. Isotope Techniques in Groundwater Hydrology 1974 (II). IAEA, Vienna, pp. 151–176.

Ward, J., Seely, M., Lancaster, N., 1983. On the antiquity of the Namib. South African Journal of Science 79, 175–183.

Wefer, G., Mulitza, S., Ratmeyer, V. (Eds.), 2004. The South Atlantic in the Late Quaternary: Reconstruction of Material Budgets and Current Systems. Springer, Berlin-Heidelberg-New York, p. 722.

Yaalon, D.H., Ward, J.D., 1982. Observations on calcrete and recent calcic horizons in relation to landforms, central Namib Desert. Palaeoecology of Africa 15, 183–186.